



Signatures of an α + core structure in $^{44}\text{Ti} + ^{44}\text{Ti}$ collisions at $\sqrt{s_{NN}} = 5.02$ TeV by a multiphase transport model

Yu-Xuan Zhang(张宇轩),¹ Song Zhang(张松) ,^{1,2,*} and Yu-Gang Ma(马余刚) ,^{1,2,†}

¹Key Laboratory of Nuclear Physics and Ion-beam Application (MOE),
Institute of Modern Physics, Fudan University, Shanghai 200433, China

²Shanghai Research Center for Theoretical Nuclear Physics, NSFC and Fudan University, Shanghai 200438, China

It is important to understand whether α -clustering structures can leave traces in ultra-relativistic heavy ion collisions. Using the modified AMPT model, we simulate three α + core configurations of ^{44}Ti in $^{44}\text{Ti} + ^{44}\text{Ti}$ collisions at $\sqrt{s_{NN}} = 5.02$ TeV as well as other systems with Woods-Saxon structures. One of these configurations has no additional constraint, but the other two have the Mott density edge r_{Mott} set as either a lower or upper bound on the cluster position r_α to check the influence of α dissolution. This is the first time that the initial stage of the geometric properties in heavy-ion collisions has been configured using the traditional treatment of the nuclear structure. We compare the radial nucleon density, multiplicity distribution, transverse momentum spectra, eccentricity, triangularity, elliptic flow and triangular flow of these six systems. α + core structures can alter all these observations especially in the most-central collisions, among which elliptic flow is the most hopeful as a probe of such structures.

I. INTRODUCTION

Predicted by quantum chromodynamics (QCD) [1], the confinement of hadronic matter may be broken under extreme conditions at high temperature or density, resulting in a new matter state called quark-gluon plasma (QGP) [2]. QGP contains deconfined quarks and gluons, providing us a chance to understand the essence of strong interaction on a new scale, which can help develop QCD further in return. Besides, the extreme conditions required by QGP are expected to exist in the early universe right after the Big Bang [3], so the investigation of QGP is also of great importance for revealing the universe origin. One of the important tools to gain such conditions is the ultra-relativistic heavy-ion collision, which is currently performed by the CERN (European Organization for Nuclear Research) Large Hadron Collider (LHC) [4–6] and the Relativistic Heavy Ion Collider (RHIC) at the Brookhaven National Laboratory [7–9]. Extensive studies are helpful in exploring the QCD phase structure and diagram [10–14]. Among the results presented by different QGP probes, particle production [15] and collectivity [16] play instrumental roles in describing the evolution of collision systems. It is widely recognized that they reflect the initial state of system and efforts to explain them usually involve modeling of the basic collision mechanism.

Recently, the influences of nuclear structure are taken into account in this community by transport or hydrodynamics models configured with initial nuclear structure [17–23]. And these works suggest that there is a potential window on investigating nuclear structure by relativistic heavy-ion collisions [24, 25]. Among various nuclear structures, the α -clustering structure inside nuclei is of particular interest. The α cluster model, first

proposed by Gamow [26], has been demonstrated to be a powerful tool in describing nuclear structure [27–29], α decay [30, 31], ground state bands [32] and so on. In this model, light nuclei could be thought to be made of α clusters as well as some nucleons or other smaller clusters [27, 33–35], while for heavy nuclei, only part of nucleons may cluster and a core could be formed by the remained nucleons [30, 32, 36]. The clustering effect is important to nuclear equations of state, nucleosynthesis and many other problems [37–40]. Various observables have therefore been proposed to study the clustering of nuclei in the heavy-ion reaction, such as collective flow [41–44], multiplicity correlation [45, 46] as well as giant resonance [38, 47–49] etc. It is still an interesting question whether such cluster structures will form signatures in ultra-relativistic heavy-ion collisions. Some review on α -clustering effects can be found in [24, 50–52]. For light nuclei, there is prediction [41, 53, 54] that clustering may lead to the variance of harmonic flow measures, implying a granular geometry preserved in ultra-relativistic heavy-ion collisions. Some positive simulation results [42, 54–56] have been reported under a multiphase transport (AMPT) model [57]. However, for heavy nuclei, behaviors of α -cluster structures remain unclear in ultra-relativistic collisions, and further investigation is required.

Among heavy nuclei, those with potential α + doubly magic core structures draw extra concentration since they match well with the binary α cluster model [32, 58] and avoid a complex many-body problem [59]. Through a modified AMPT model, we test this cluster model by simulating $^{44}\text{Ti} + ^{44}\text{Ti}$ collisions at $\sqrt{s_{NN}} = 5.02$ TeV with α + core (α + c) or Woods-Saxon (W-S) structures. We analyze the influence of this mode on yields and harmonic flow of major charged particles (π^\pm , K^\pm , p , \bar{p}) and find possible signatures related to the α + ^{40}Ca structure. Sec. II presents our approaches to acquiring the α + core simulation and analyzing the results. Re-

* Email: song_zhang@fudan.edu.cn

† Email: mayugang@fudan.edu.cn

sults and discussion are shown in Sec. III, and the last section is the conclusion.

II. METHODOLOGY

The AMPT model is a hybrid transport model aimed at simulating heavy ion collisions at RHIC and LHC energy [57, 60]. It contains several sub-models, such as the heavy-ion jet interaction generator (HIJING) model [61], Zhang's parton cascade (ZPC) model [62], the Lund JETSET fragmentation model [63, 64], a quark coalescence model and a relativistic transport (ART) model [65]. In our work, heavy-ion collisions at the center of mass energy $\sqrt{s_{NN}} = 5.02$ TeV will reach ultra-high temperature, leading to high QGP formation possibility. Hence, a string-melting version of the AMPT model is chosen for our simulation. In this model version, all excited strings are fragmented into partons and hadronized together with minijet partons, which is closer to the QGP case.

In the AMPT model, the initial conditions of the collisions are provided by the HIJING model, where projectile and target nuclei are shaped into Woods-Saxon distributions and then the positions of constituent nucleons are set event by event. A 3-parameter Fermi function of the position \mathbf{r} is used to describe Woods-Saxon distributions:

$$f(r) = A \frac{1 + \omega r^2 / c^2}{1 + \exp[(r - c)/z]}. \quad (1)$$

Here A is the normalization factor, c is the radius parameter, z is the diffusion parameter, and ω is the newly added third parameter. If $\omega < 0$, this function is cut off at $1 + \omega r^2 / c^2 = 0$. For ^{40}Ca , there are optimized parameters preset in the HIJING model, while for ^{44}Ti , only automatically fitted data is available. ^{50}Ti , a natural nuclei with a neutron magic number $N = 28$, is considered as a singly closed shell core in the binary α cluster model [66] and also not preset in the HIJING model. We additionally include it in our simulation to evaluate this fitting and test the system size effects.

Instead of fixed cluster configurations common in light nucleus research [42, 54], a non-localized $\alpha + ^{40}\text{Ca}$ structure is introduced to modify the initial conditions by using the local potential model (LPM) [30, 67]. This structure features global motion of clusters and has well described the alpha condensate state of light nuclei like ^{12}C [68] and the $\alpha + \text{core}$ structure of heavy nuclei such as ^{20}Ne [69] and ^{212}Po [59]. In LPM, we utilize the cluster position r_α [30, 67] to describe the α cluster potential $V(\mathbf{r}_\alpha)$, which can be divided into the Coulomb potential $V_C(r_\alpha)$, the centrifugal potential $V_L(r_\alpha)$, and the nuclear potential $V_N(\mathbf{r}_\alpha)$. With a uniformly charged spherical

core assumption, $V_C(r_\alpha)$ can be written as

$$V_C(r_\alpha) = \begin{cases} \frac{Z_\alpha Z_c e^2}{2R} \left(3 - \frac{r_\alpha^2}{R^2} \right), & r_\alpha < R \\ \frac{Z_\alpha Z_c e^2}{r_\alpha}, & r_\alpha \geq R \end{cases} \quad (2)$$

where Z_α and Z_c are the charge numbers of the α cluster and the core, and R is the core radius decided later by fitting $V_N(\mathbf{r}_\alpha)$. The form of $V_L(r_\alpha)$ is

$$V_L(r_\alpha) = \frac{\hbar^2}{2\mu_\alpha r_\alpha^2} L(L+1), \quad (3)$$

with L the azimuthal quantum number and μ_α is the reduced mass in α two-body systems. Here we suppose that projectile and target nuclei are at their ground states, so L is equal to zero and $V_L(r_\alpha)$ can be neglected. As for $V_N(\mathbf{r}_\alpha)$, we select a $(1 + \text{Gaussian}) \times (\text{W.S.} + \text{W.S.}^3)$ potential model [58], with which $V_N(\mathbf{r}_\alpha)$ can be simply decided by the length r_α . In this model there is

$$V_N(r_\alpha) = -V_0 \left(1 + \lambda e^{-r_\alpha^2/\sigma^2} \right) \left\{ \frac{b}{1 + e^{(r_\alpha - R)/a}} + \frac{1 - b}{[1 + e^{(r_\alpha - R)/3a}]^3} \right\}, \quad (4)$$

where V_0 , λ , a and b are fixed parameters, R and σ are free parameters for fitting. Here these parameters are the same as in Ref. [58], which well describes the ground state bands of ^{44}Ti . Specifically, we set $V_0 = 220$ MeV, $a = 0.65$ fm, $b = 0.3$, $\lambda = 0.14$, $R = 4.551$ fm, and $\sigma = 0.425$ fm. Then with α decay energy $E_\alpha = -5.1271$ MeV [70], we can gain the cluster's radial wave function $\varphi_L(r_\alpha)$ by numerically solve its stationary Schrödinger equation. Figure 1 (a) shows the normalized radial component of the cluster wave function $f_L(r_\alpha) = \varphi_L(\mathbf{r}_\alpha) r_\alpha / Y_{LM}(\theta, \phi)$. The probability density of r_α can be gained from $\rho(r_\alpha) = |f_L(r_\alpha)|^2$ and the corresponding cumulative distribution function $F_L(r_\alpha)$ is presented in Fig. 1 (b).

With $F_L(r_\alpha)$, we are able to insert an α cluster before core nucleons are placed. In the binary α cluster model, external influence on cluster or core nucleons is usually neglected, so here both α clusters and ^{40}Ca cores have Woods-Saxon inner structures, and their parameters are simply decided by the HIJING preset data. For α , it means $c = 0.964$ fm, $z = 0.322$ fm, and $\omega = 0.517$ in Eq. (1). For ^{40}Ca , there is $c = 3.766$ fm, $z = 0.586$ fm, and $\omega = -0.161$. According to Ref. [59], the Pauli blocking may lead to the dissolution of α clusters at the Mott density $\rho_{\text{Mott}} = 0.02917$ fm $^{-3}$, which is $r_{\text{Mott}} = 4.498$ fm for ^{40}Ca . This Mott density of a nucleus is given by the maximum density at which a nucleus of zero momentum can still be bound [71, 72]. That is to say, α clusters may not always exist in the $\alpha + \text{core}$ nuclei even if the model fully matches the reality. As pointed out in Refs. [30, 73, 74], the α cluster preformation probability P_α can be estimated by calculating its distribution outside r_{Mott} . And according to these references, P_α usually has

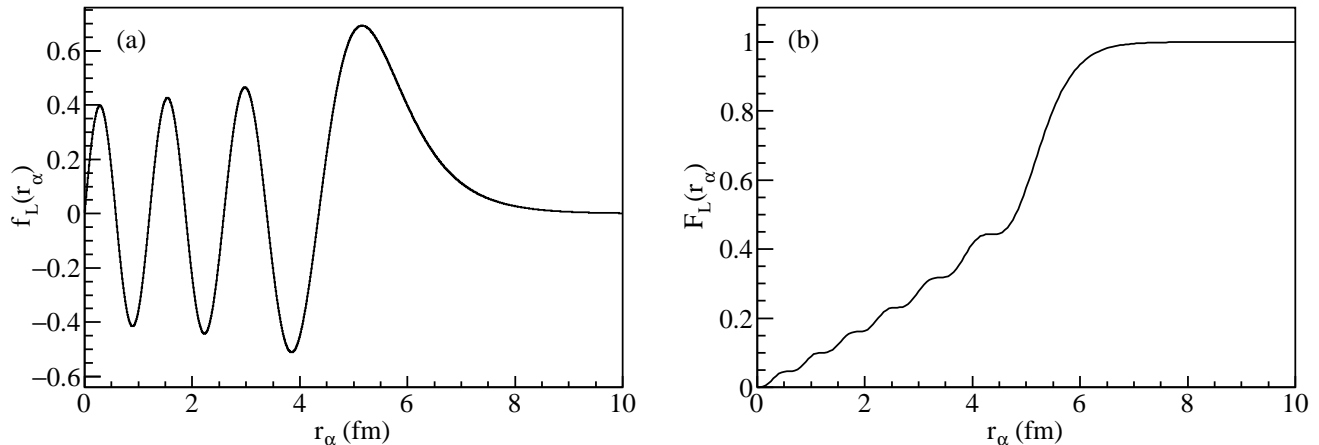


FIG. 1. The normalized radial component $f_L(r_\alpha)$ of the α cluster wave function for ^{44}Ti at the ground state (a) and the cumulative r_α distribution function $F_L(r_\alpha)$ (b).

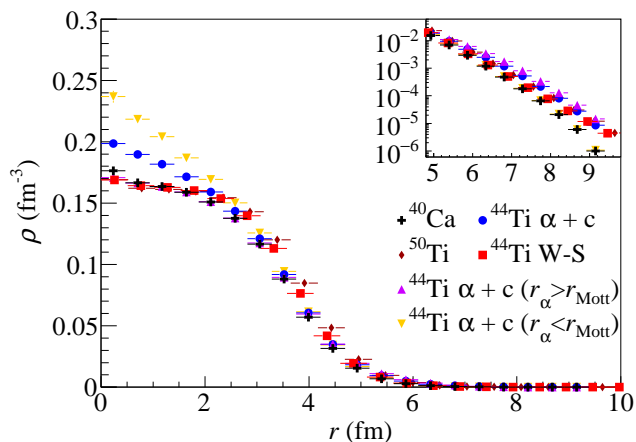


FIG. 2. The nucleon density ρ of projectile and target nuclei shown linearly in the main graph and logarithmically in the top right as a function of the distance r .

a magnitude of a few tenths, which can be high enough to form observable alteration. Shown in Fig. 1 (b), about 55% of clusters are in $r_\alpha > r_{\text{Mott}}$ for the classical binary cluster model, which is acceptable considering the existing results. Since the clustering state is not completely dominant, we also test the influence of cluster dissolution by cutting off r_α at r_{Mott} like in P_α estimation in addition to the widely adopted no dissolution case. Though $r_\alpha < r_{\text{Mott}}$ case results in the breaking of the nuclear matter saturation as discussed following, the simulation can be a comparison for α cluster effect with other cases.

To characterize the initial geometry, we utilize the eccentricity ε_n of participant partons and the anisotropic flow v_n of final charged particles. ε_n is a direct description of spatial anisotropy. In specific heavy-ion collision,

it can be defined as [55]

$$\varepsilon_n = \frac{\sqrt{\langle r^n \cos(n\varphi_{part}) \rangle^2 + \langle r^n \sin(n\varphi_{part}) \rangle^2}}{\langle r^n \rangle}, \quad (5)$$

where φ_{part} is the azimuthal angle and r the position. ε_2 is usually called eccentricity and ε_3 is called triangularity. $\langle \dots \rangle$ denotes average over participant nucleons here, but later $\langle \varepsilon_n \rangle$ means average over events. Hydrodynamics demonstrates a picture that the initial asymmetry in coordinate space will transfer to the final momentum space [75]. And we should point out the initial geometry asymmetry in the collisions includes the intrinsic structures and the overlapped region of the colliding nuclei, as well as fluctuation. In actual collision experiments, the participant parton positions are undetectable due to quark confinement, so description from collective flow reflecting anisotropy of particles at the final state is also necessary. On the other hand, the investigation of the final momentum space will disclose the properties of the initial stage and in further the intrinsic structure of nuclei.

The anisotropic components of collective flow can be characterized by the Fourier expansion of particle momentum distribution [76–81]:

$$E \frac{d^3N}{d^3p} = \frac{1}{2\pi} \frac{d^2N}{p_T dp_T dy} \left\{ 1 + \sum_{n=1}^{\infty} 2v_n \cos[n(\varphi - \Psi_n)] \right\}. \quad (6)$$

Here E is the particle energy, p_T is the transverse momentum, and y is the rapidity. The Fourier expansion coefficient v_n is the n -th order of the anisotropic flow and Ψ_n is the corresponding event plane angle. Among all orders of flow, the elliptic flow v_2 and the triangular flow v_3 draw extra attention since they represent the initial collision geometry and its fluctuations, respectively [82]. A common way to extract anisotropic flow is the cumulant method [83], which allows us to

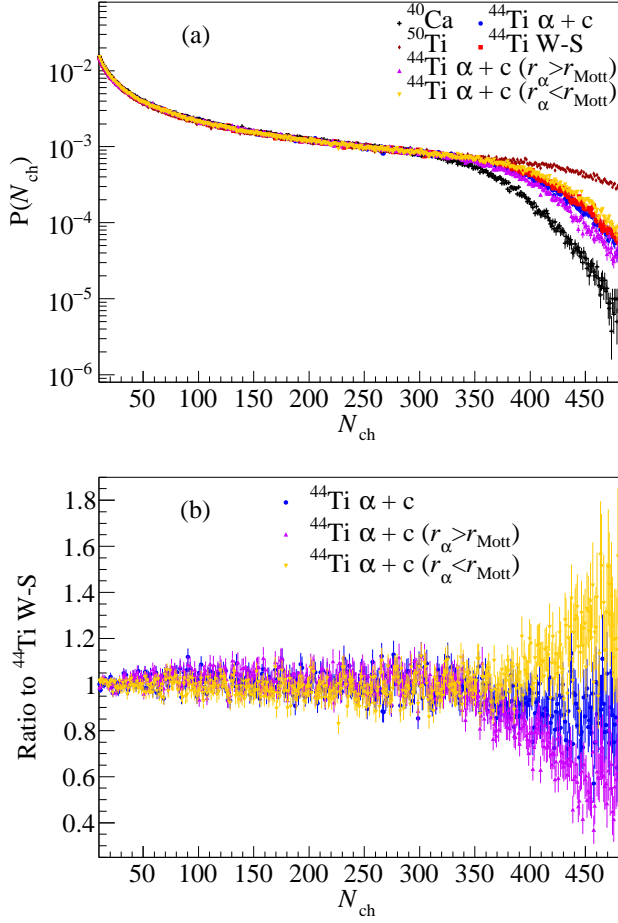


FIG. 3. The multiplicity distribution of major charged particles within $|\eta| < 0.5$ (a) and ratios to the Woods-Saxon structure in $^{44}\text{Ti} + ^{44}\text{Ti}$ systems (b).

build multi-particle azimuthal correlations without looping over all particle multiplets. In a two sub-event case, with $Q_n = \sum_{i=1}^M e^{in\varphi_i}$ storing the azimuthal angle information of M particles, the two-particle correlation and its average over all events in this method can be written as [84]

$$\begin{aligned} \langle 2 \rangle_{a|b} &= \frac{Q_{n,a} Q_{n,b}^*}{M_a M_b}, \\ \langle \langle 2 \rangle \rangle_{a|b} &= \frac{\sum_{events} M_a M_b \langle 2 \rangle_{a|b}}{\sum_{events} M_a M_b}, \end{aligned} \quad (7)$$

where a and b are symbols for these two sub-events. The corresponding n -th order flow can be written as

$$v_n^{a|b} \{2\} = \sqrt{c_n^{a|b} \{2\}} = \sqrt{\langle \langle 2 \rangle \rangle_{a|b}}, \quad (8)$$

where $c_n^{a|b} \{2\}$ is the two-particle cumulant. Here we assume the flow in two sub-events is the same, which is reasonable in a symmetric system with the same sub-event kinetic windows.

We can also generate two-particle correlation directly to extract collective flow [82, 85, 86]. For trigger-associated particle correlation, we can go over all particle pairs and gain a per-trigger-particle associated yield,

$$\begin{aligned} \frac{1}{N_{trig}} \frac{d^2 N^{pair}}{d\Delta\eta d\Delta\varphi} &= B(0,0) \frac{S(\Delta\varphi, \Delta\eta)}{B(\Delta\varphi, \Delta\eta)}, \\ S(\Delta\varphi, \Delta\eta) &= \frac{1}{N_{trig}} \frac{d^2 N^{same}}{d\Delta\varphi d\Delta\eta}, \\ B(\Delta\varphi, \Delta\eta) &= \frac{1}{N_{trig}} \frac{d^2 N^{mix}}{d\Delta\varphi d\Delta\eta}, \end{aligned} \quad (9)$$

where $\Delta\varphi$ and $\Delta\eta$ are the differences in φ and pseudorapidity η of the pair, and N_{trig} is the trigger particle yield. $S(\Delta\varphi, \Delta\eta)$ is the per-trigger-particle pair yield in the same event. $B(\Delta\varphi, \Delta\eta)$ is generated by pairing trigger particles with associated particles from other events. The Fourier expansion of associated yields is

$$\frac{1}{N_{trig}} \frac{dN^{pair}}{d\Delta\varphi} = \frac{N_{asso}}{2\pi} \left[1 + \sum_{n=1}^{\infty} 2V_{n\Delta} \cos(n\Delta\varphi) \right], \quad (10)$$

where $V_{n\Delta}$ is the coefficient and N_{asso} is the associated particle yield. With non-flow correlation reduced, there is

$$V_{n\Delta} = v_n^{asso} v_n^{trig}, \quad (11)$$

and

$$v_n^{corr} = \sqrt{V_{n\Delta}} \quad (v_n^{asso} = v_n^{trig}), \quad (12)$$

where v_n^{asso} , v_n^{trig} and v_n^{corr} are the flow of associated particles, triggers, and the entire correlation system respectively. In practice a $\Delta\eta$ gap is applied to Eq.(9) while projected into one-dimensional correlation function of Eq.(10), which is considered to reduce non-flow effectively.

III. RESULT AND DISCUSSION

In this work, three collision systems of Woods-Saxon nuclei and three of $\alpha + \text{core}$ ^{44}Ti are simulated by the string-melting AMPT model version 2.26t7b. The first three systems are $^{50}\text{Ti} + ^{50}\text{Ti}$, $^{40}\text{Ca} + ^{40}\text{Ca}$, and $^{44}\text{Ti} + ^{44}\text{Ti}$. In other three systems, one has no r_α constraint, one follows $r_\alpha > r_{Mott}$, and the last one follows $r_\alpha < r_{Mott}$. Each system has 8×10^5 events, which are uniformly divided into ten centrality classes according to the multiplicity of major charged particles within $p_T > 0.2$ GeV/c and $|\eta| < 0.5$ (N_{ch}).

To assess the initialization configuration, we first extract the radial nucleon density of projectile and target nuclei, which is presented in Fig. 2. The central nucleon density is almost the same for Woods-Saxon ^{40}Ca , ^{50}Ti and ^{44}Ti , showing typical nuclear matter saturation. However, this feature is broken for nuclei with a classical $\alpha + \text{core}$ structure. Further density increase appears

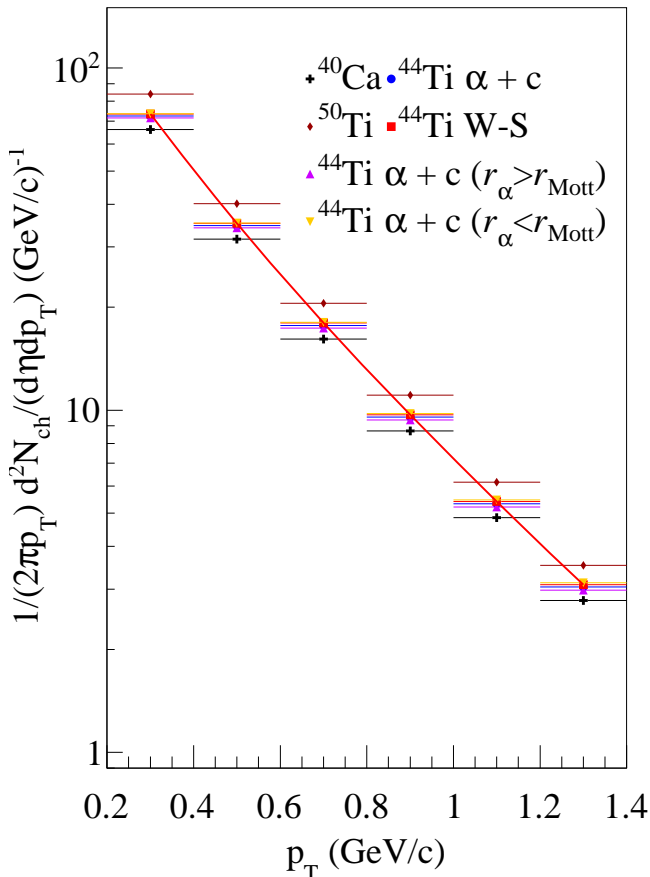


FIG. 4. The transverse momentum spectra of major charged particles within $|\eta| < 0.5$ for integrating all centralities. The red line connected with red squares is plotted for the case of W-S as a baseline for comparing other $^{44}\text{Ti} + ^{44}\text{Ti}$ systems. The same situation is presented in following figures.

for $r_\alpha < r_{\text{Mott}}$, while for $r_\alpha > r_{\text{Mott}}$, the saturation is restored, indicating that this breaking is due to clusters neglecting Pauli blocking. This negligence widely exists in energy level calculation, where the result is mainly drawn from stationary Schrödinger equations regardless of the cluster dissolution [58, 67]. Some progress has been made in Ref. [69], where cluster motion avoids mutual overlap due to the Pauli blocking effect. However, this just falls in the $r_\alpha > r_{\text{Mott}}$ case and the cluster dissolution is not directly handled. So future optimization to introduce such transition is still necessary in relative areas. Another difference is in the peripheral area. For Woods-Saxon nuclei, the nucleon density decreases exponentially in peripheral areas, but for $\alpha + \text{core}$ structures, the clusters introduce another density enhancement. This time the Mott density constraint concentrates more clusters outside and hence leads to higher peripheral density than the classical cluster model's.

Seeing such density distribution differences, we expect

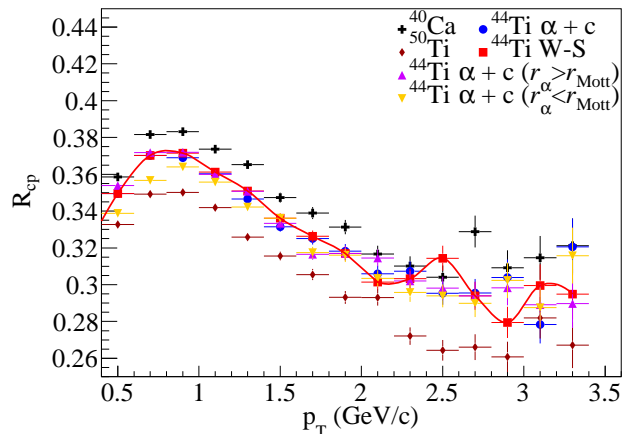


FIG. 5. The nuclear modification factor R_{CP} of the centrality class 0-10% as a function of p_T . The centrality class 80-90% is the denominator.

alteration related to nuclear structures in particle production. Fig. 3 (a) reports the probability distribution of N_{ch} as $P(N_{\text{ch}})$. Distributions of all systems look alike at low N_{ch} , reflecting the low possibility of clusters appearing in collision zones and similar surface behaviors of Woods-Saxon nuclei or cores. But when N_{ch} is high, the influence of nuclear structures starts to play an important role in the multiplicity distribution. A $P(N_{\text{ch}})$ ratio comparison is presented for $^{44}\text{Ti} + ^{44}\text{Ti}$ systems in Fig. 3 (b), where clear depression is seen in $r_\alpha > r_{\text{Mott}}$ at high N_{ch} , while enhancement is shown instead when $r_\alpha < r_{\text{Mott}}$. The mixed result of free α tends to decrease slightly since there are a bit more clusters outside the cores as discussed in Sec. II. We also present the transverse momentum spectra of major charged particles within $|\eta| < 0.5$ for integrating all centralities in Fig. 4, in which the red line connected with red squares is plotted for the case of W-S as a baseline (the same in the following figures). The distinction due to nuclear structures is rather small but still exists this time, which is consistent with Fig. 3 (b) where the deviation only appears in the ultra-high N_{ch} events and is lower than one order of magnitude. This behaviour is similar to the multiplicity distribution and ratio in isobar collisions [22, 87] while considering the neutron skin effect.

To further look into this phenomenon, we introduce the nuclear modification factor R_{CP} , which can be defined as [88]

$$R_{\text{CP}} = \frac{d^2 N_{\text{ch}}^{\text{cent}} / (dp_T dy) / \langle N_{\text{coll}}^{\text{cent}} \rangle}{d^2 N_{\text{ch}}^{\text{peri}} / (dp_T dy) / \langle N_{\text{coll}}^{\text{peri}} \rangle}. \quad (13)$$

Here $\langle N_{\text{coll}} \rangle$ is the average inelastic binary collision number over events. The superscript “cent” represents central collisions and “peri” means peripheral events. R_{CP} is usually used to estimate the particle production suppression, and is widely considered to be negatively

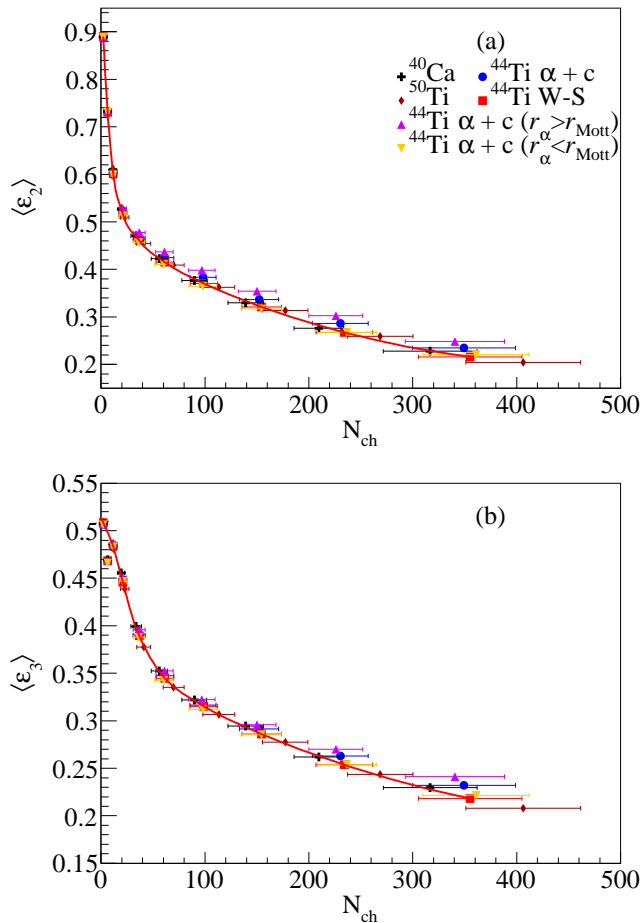


FIG. 6. Eccentricity (a) and triangularity (b) of participant partons as a function of N_{ch} .

correlated with multiplicity. Figure 5 shows the R_{CP} results of the centrality class 0-10% with the class 80-90% as the denominator. The $^{40}\text{Ca} + ^{40}\text{Ca}$ system shows the highest R_{CP} , while $^{50}\text{Ti} + ^{50}\text{Ti}$ has the lowest, reflecting typical multiplicity correlation. Among $^{44}\text{Ti} + ^{44}\text{Ti}$ systems, in the low p_T range the difference caused by nuclear structures is more significant than in Fig. 4, which is also negatively correlated with the multiplicity. At other p_T , R_{CP} is almost the same for all $^{44}\text{Ti} + ^{44}\text{Ti}$ systems. Unfortunately, such difference is still far from distinguishing itself compared with the system size influence.

Another issue about the initialization configuration is the collision zone shape, which can be characterized by ε_n defined in Eq. (5). Fig. 6 presents $\langle \varepsilon_2 \rangle$ and $\langle \varepsilon_3 \rangle$ of participant partons in all centrality classes as a function of N_{ch} . $\langle \varepsilon_2 \rangle$ and $\langle \varepsilon_3 \rangle$ decrease with the increasing of N_{ch} in these collision systems, which presents a system size dependence like that in our previous work [89]. For Woods-Saxon nuclei, their eccentricity follows an order of multiplicity, implying that for similar systems ε_n is mainly affected by the system size. For cluster + core nuclei, at low N_{ch} the eccentricity is almost the same as

for the Woods-Saxon structure, while at high N_{ch} an eccentricity enhancement appears when α clusters are in $r_\alpha > r_{\text{Mott}}$ or have no r_α constraint. The enhancement is stronger in $r_\alpha > r_{\text{Mott}}$, suggesting that it is α clusters outside the cores that cause this ε_n enhancement. These behaviors of ε_n also match the analysis of particle production above, where the influence of cluster + core structures plays an important role in high multiplicity events but diminishes in peripheral collisions. Interestingly, the α -cluster structure effects on the eccentricity are consistent with our previous investigations [42, 54] for $^{12}\text{C} + ^{12}\text{C}$ and $^{16}\text{O} + ^{16}\text{O}$ collisions where the chain structure enhances ε_2 and reduces ε_3 and the triangle or tetrahedron structure do the opposite. This implies that the nuclear intrinsic structure plays an important role in the geometry shape formation at the collision initial stage.

Figure 7 shows the elliptic flow and the triangular flow of major charged particles gained with two sub-event cumulants or direct two-particle correlation. For the two sub-event cumulant method, the kinetic window is $-2.4 < \eta_a < 0$, $0 < \eta_b < 2.4$ and $0.3 < p_T < 4.0$ GeV/c, where η_a and η_b are the pseudorapidity of particles in sub-events a and b, respectively. For direct two-particle correlation, the kinetic window of the trigger and associated particles is $0.3 < p_T < 4.0$ GeV/c and $-2.4 < \eta < 2.4$, so that the measurement involves the same particles as in the two sub-event cumulant method. A pseudorapidity gap $\Delta\eta > 2.0$ is required for effective correlation to avoid non-flow effects. The result of peripheral events in centrality 60–100% is omitted since jet-like correlation is the main source of v_2 , and v_3 here. In Fig. 7 (a) $v_2^{a|b}\{2\}$ shows obvious enhancement for cluster + core structures except in $r_\alpha < r_{\text{Mott}}$, while in Fig. 7 (b) $v_3^{a|b}\{2\}$ of all systems follows similar multiplicity order except in the highest multiplicity class. In Fig. 7 (c) and (d), the results of v_2^{corr} and v_3^{corr} show great similarity with $v_2^{a|b}\{2\}$ and $v_3^{a|b}\{2\}$, showing that the difference between v_2 and v_3 is independent of the exact tool to extract the flow.

To carry out further investigation, we try a new perspective of the flow-to-eccentricity ratio. Hydrodynamic calculations [75, 90] point out that there is a proportional relationship between ε_n and v_n for $n = 2, 3$, so their ratio might be able to reflect the efficiency to transform initial geometry asymmetry to final momentum space asymmetry [42]. The ratios of $v_n^{a|b}\{2\}$ to $\langle \varepsilon_n \rangle$ are shown in Fig. 8. Although the behaviors of $v_2^{a|b}\{2\}$ and $v_3^{a|b}\{2\}$ are quite different, their ratios to corresponding eccentricity do share the same pattern. Like the case of $\langle \varepsilon_n \rangle$, $v_n^{a|b}\{2\}/\langle \varepsilon_n \rangle$ of Woods-Saxon systems follows the order of multiplicity, while for core + cluster nuclei, $v_n^{a|b}\{2\}/\langle \varepsilon_n \rangle$ shows influence of nuclear structures at high N_{ch} except in $r_\alpha < r_{\text{Mott}}$. This time binary structures lead to a slight depression, indicating that the cluster effects may be weakened by particle interaction during collisions to some extent. Combining $\langle \varepsilon_n \rangle$, $v_n^{a|b}\{2\}$ and

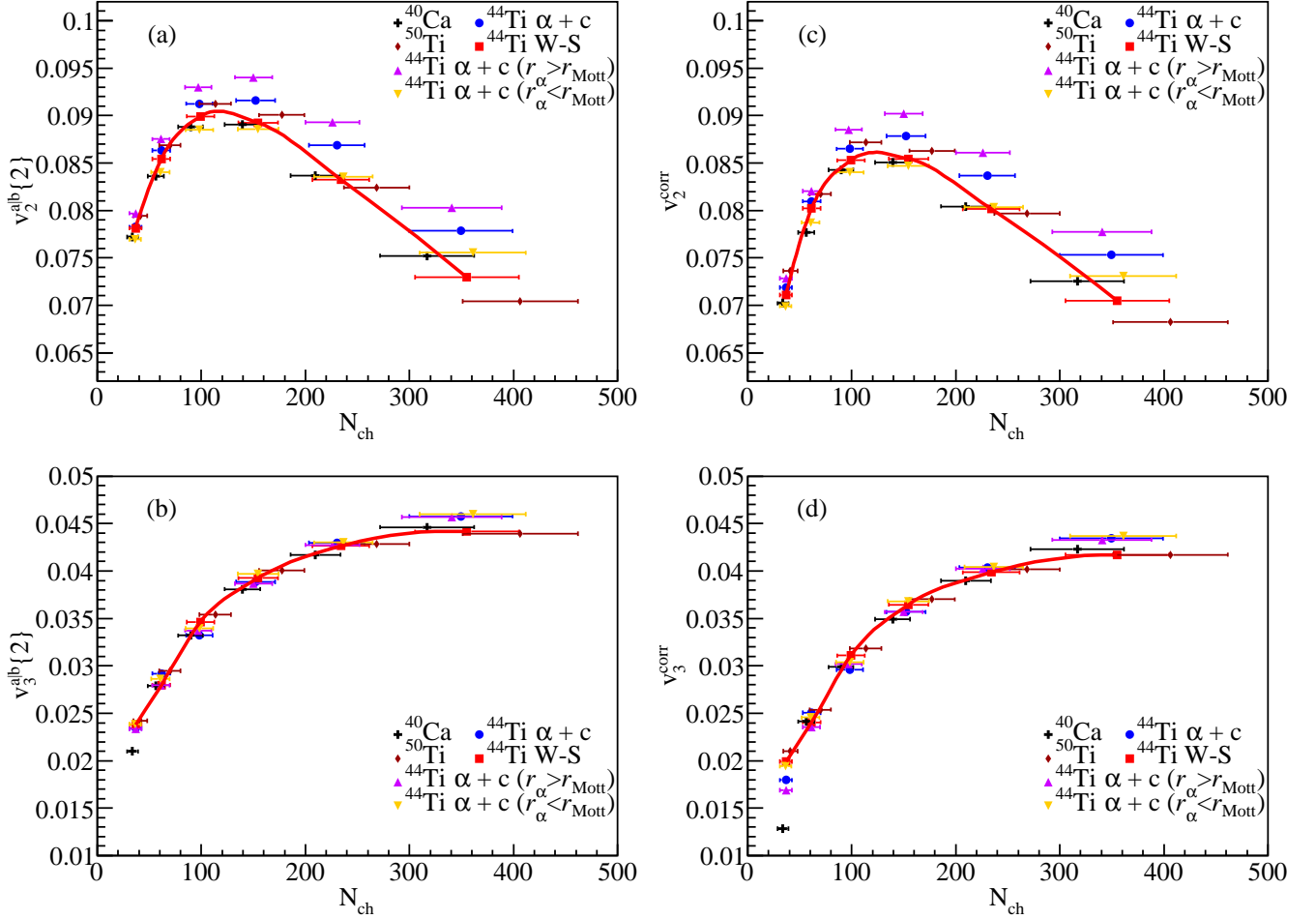


FIG. 7. The elliptic flow and triangular flow by the two sub-event cumulant method or by the direct two-particle correlation method as a function of N_{ch} . (a) and (b) are $v_2^{alb}\{2\}$ and $v_3^{alb}\{2\}$ by the two sub-event cumulant method, and (c) and (d) are v_2^{corr} and v_3^{corr} by the direct two-particle correlation method.

$v_n^{alb}\{2\}/\langle\varepsilon_n\rangle$, we can say that the different behaviors between v_2 and v_3 are likely to be the natural result of system evolution.

To investigate the kinetic window dependence of the influence of α -cluster nuclear structure, the p_T -differential $v_n^{alb}\{2\}$ of the centrality class 0-10% is calculated and shown in Figure 9. $v_2^{alb}\{2\}$ and $v_3^{alb}\{2\}$ increase with the increasing of p_T and reach the maximum around $p_T \sim 2.5$ GeV/c, and then present a decreasing trend. The core + cluster enhancement is still obvious this time for $v_2^{alb}\{2\}$, while $v_3^{alb}\{2\}$ remains similar for all six systems. So the α -cluster nuclear structure effect on collective flow does not depend on the selected p_T window and p_T -differential collective flow may also be a good probe for nuclear structures.

From the above analysis of the differential flow in the most-central collisions and the N_{ch} dependence of flow, it is shown that elliptic flow coefficients in the natural nucleus collision systems, $^{50}\text{Ti} + ^{50}\text{Ti}$, $^{44}\text{Ti}(\text{W-S}) +$

$^{44}\text{Ti}(\text{W-S})$, $^{40}\text{Ca} + ^{40}\text{Ca}$, follow the order of $v_2(^{40}\text{Ca}) > v_2(^{44}\text{Ti}(\text{W-S})) > v_2(^{50}\text{Ti})$ which is consistent with our previous study of the system size dependence of collective flow [89]. And it is obvious that $^{44}\text{Ti} + ^{44}\text{Ti}$ configured with α -clusters is significantly biased against the order of v_2 in the natural nucleus collision systems, up to 10%, no matter whether the Mott density is taken into account for ^{44}Ti . In the experiment, a system scan of relativistic heavy-ion collisions near ^{44}Ti could be considered as a probe to explore the signature of the α -cluster structure in ^{44}Ti .

IV. CONCLUSION

In this work, we test the influence of α cluster + core structures on particle production and collectivity in $^{44}\text{Ti} + ^{44}\text{Ti}$ collisions at $\sqrt{s_{NN}} = 5.02$ TeV with the AMPT model where the initial geometry properties is configured by using the traditional treatment method of the nuclear

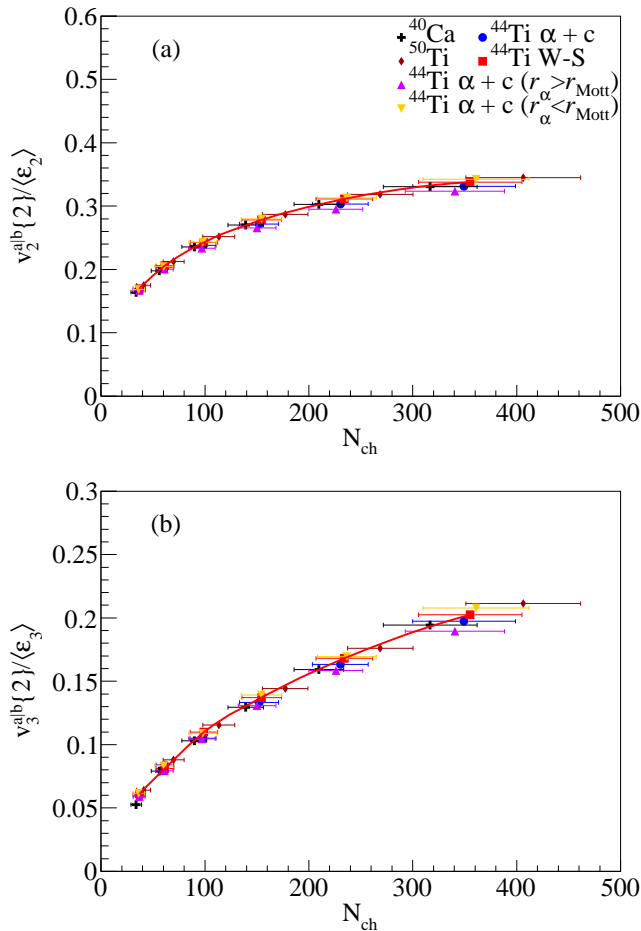


FIG. 8. Ratios of $v_2^{alb}\{2\}$ to $\langle \varepsilon_2 \rangle$ (a) and $v_3^{alb}\{2\}$ to $\langle \varepsilon_3 \rangle$ (b) as a function of N_{ch} .

structure. Due to α dissolution, there might be the so-called Mott density restricting the positions of α clusters. So we try three modes of binary structures, which are $r_\alpha < r_{\text{Mott}}$, $r_\alpha > r_{\text{Mott}}$ and free r_α . For real nuclei, only the last two are possible. The absence of α dissolution greatly increases central nucleon density and leads to the breaking of nuclear matter saturation, implying the necessity of including Mott density in future $\alpha + \text{core}$ structure research. Clusters outside cores also raise the peripheral nucleon density but to a much smaller degree.

In particle production, the structure influence mainly contributes to high multiplicity events. Systems with clusters inside cores show a higher fraction of high N_{ch} events, and clusters outside cores lead to the contrary. The mixed mode is similar to the Woods-Saxon situation, with a much weaker enhancement at high N_{ch} . The alteration is less than one order of magnitude, so it is hard to detect binary structures in transverse momentum spectra. We also calculate the nuclear modification factor R_{CP} in the centrality class 0-10% and found that the signal is stronger, but still not enough to decide the structure. The initial geometry is also affected by clus-

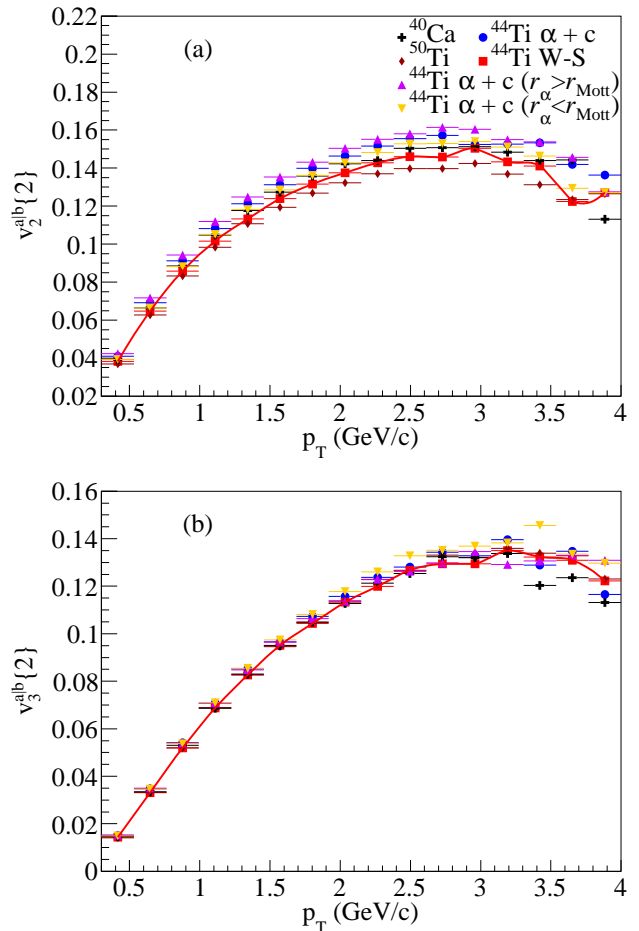


FIG. 9. $v_2^{alb}\{2\}$ (a) and $v_3^{alb}\{2\}$ (b) as a function of p_T in the centrality class 0-10%.

ter + core structures. Both ε_2 and ε_3 are increased by clusters outside cores, while clusters inside seem to have no effect. The difference in v_2 is strengthened in comparison with ε_2 , so there may be possibility to distinguish the binary structure with a cross-check of elliptic flow in similar systems. However, in v_3 the difference almost vanishes due to system evolution, leaving traces only in central events.

Although it is still under debate whether α cluster structures can generate strong signatures in ultra-relativistic heavy-ion collisions, there have been many predictions about the all-cluster structures. Our result provides a new insight of $\alpha + \text{core}$ structures into this issue, showing that elliptic flow might be a good probe of binary structures, while triangular flow and particle production are less sensitive to these structures. And a system scan of relativistic heavy-ion collisions is proposed to be performed in the experiment to investigate $\alpha + \text{core}$ structures through the system dependence of elliptic flow.

ACKNOWLEDGMENTS

This work was supported in part by National Key R&D Program of China under Grant No. 2018YFE0104600 and 2016YFE0100900, the National Natural Science Foundation of China under contract Nos. 12275054, 12147101, 11925502, 11890710, 11890714, 12061141008

and 11875066, the Strategic Priority Research Program of CAS under Grant No. XDB34000000, the Guangdong Major Project of Basic and Applied Basic Research No. 2020B0301030008, Shanghai Special Project for Basic Research No. 22TQ006 and the STCSM under Grant No. 23590780100.

-
- [1] A. Andronic, P. Braun-Munzinger, K. Redlich, and J. Stachel, Decoding the phase structure of QCD via particle production at high energy, *Nature* **561**, 321 (2018).
- [2] E. Shuryak, Quark-gluon plasma and hadronic production of leptons, photons and psions, *Phys. Lett. B* **78**, 150 (1978).
- [3] D. Boyanovsky, H. de Vega, and D. Schwarz, Phase Transitions in the Early and Present Universe, *Annu. Rev. Nucl. Part. Sci.* **56**, 441 (2006).
- [4] L. Evans and P. Bryant, LHC Machine, *J. Instrum.* **3** (08), S08001.
- [5] S. Acharya *et al.* (ALICE Collaboration), Multiplicity dependence of π , K, and p production in pp collisions at $\sqrt{s} = 13$ TeV, *Eur. Phys. J. C* **80**, 693 (2020).
- [6] B. Abelev *et al.* (ALICE Collaboration), Multiplicity dependence of pion, kaon, proton and lambda production in p-Pb collisions at $\sqrt{s_{NN}}=5.02$ TeV, *Phys. Lett. B* **728**, 25 (2014).
- [7] M. Harrison, T. Ludlam, and S. Ozaki, RHIC project overview, *Nucl. Instrum. Methods Phys. Res., Sect. A* **499**, 235 (2003).
- [8] K. Adcox *et al.* (PHENIX Collaboration), Centrality Dependence of Charged Particle Multiplicity in Au-Au Collisions at $\sqrt{s_{NN}} = 130$ GeV, *Phys. Rev. Lett.* **86**, 3500 (2001).
- [9] B. B. Back *et al.* (PHOBOS Collaboration), Energy Dependence of Particle Multiplicities in Central Au + Au Collisions, *Phys. Rev. Lett.* **88**, 022302 (2001).
- [10] A. Bzdak, S. Esumi, V. Koch, J. F. Liao, M. Stephanov, and N. Xu, Mapping the phases of quantum chromodynamics with beam energy scan, *Phys. Rep.* **853**, 1 (2020).
- [11] E. Laermann and O. Philipsen, Lattice QCD at finite temperature, *Ann. Rev. Part. Nucl. Sci.* **53**, 163 (2023).
- [12] G. Qin, 3D wakes on the femtometer scale by supersonic jets, *Nucl. Sci. Tech.* **34**, 22 (2023).
- [13] K. Sun, L. Chen, C. M. Ko, F. Li, J. Xu, and X. Zhangbu, Light nuclei production and QCD phase transition in heavy-ion collisions, *Nucl. Tech. (in Chinese)* **46**, 040012 (2023).
- [14] Q. Chen, G.-L. Ma, and J.-H. Chen, Transport model study of conserved charge fluctuations and QCD phase transition in heavy-ion collisions, *Nucl. Tech. (in Chinese)* **46**, 040013 (2023).
- [15] S. S. Adler *et al.* (PHENIX Collaboration), Identified charged particle spectra and yields in Au + Au collisions at $\sqrt{s_{NN}} = 200$ GeV, *Phys. Rev. C* **69**, 034909 (2004).
- [16] H. G. Ritter and R. Stock, Collective flow of QCD matter: a historical introduction, *J. Phys. G: Nucl. Part. Phys.* **41**, 124002 (2014).
- [17] G. Giacalone, Observing the Deformation of Nuclei with Relativistic Nuclear Collisions, *Phys. Rev. Lett.* **124**, 202301 (2020).
- [18] G. Giacalone, Constraining the quadrupole deformation of atomic nuclei with relativistic nuclear collisions, *Phys. Rev. C* **102**, 024901 (2020).
- [19] J. Jia, G. Giacalone, and C. Zhang, Separating the Impact of Nuclear Skin and Nuclear Deformation in High-Energy Isobar Collisions, *Phys. Rev. Lett.* **131**, 022301 (2023).
- [20] J. Jia, Probing triaxial deformation of atomic nuclei in high-energy heavy ion collisions, *Phys. Rev. C* **105**, 044905 (2022).
- [21] H. Li, H.-j. Xu, Y. Zhou, X. Wang, J. Zhao, L.-W. Chen, and F. Wang, Probing the Neutron Skin with Ultrarelativistic Isobaric Collisions, *Phys. Rev. Lett.* **125**, 222301 (2020).
- [22] F. Li, Y.-G. Ma, S. Zhang, G.-L. Ma, and Q. Shou, Impact of nuclear structure on the background in the chiral magnetic effect in $^{96}_{44}\text{Ru} + ^{96}_{44}\text{Ru}$ and $^{96}_{40}\text{Zr} + ^{96}_{40}\text{Zr}$ collisions at $\sqrt{s_{NN}} = 7.7 - 200$ GeV from a multiphase transport model, *Phys. Rev. C* **106**, 014906 (2022).
- [23] X.-L. Zhao and G.-L. Ma, Search for the chiral magnetic effect in collisions between two isobars with deformed and neutron-rich nuclear structures, *Phys. Rev. C* **106**, 034909 (2022).
- [24] Y.-G. Ma and S. Zhang, Influence of nuclear structure in relativistic heavy-ion collisions, in *Handbook of Nuclear Physics*, edited by I. Tanihata, H. Toki, and T. Kajino (Springer Nature Singapore, Singapore, 2020) pp. 1–30.
- [25] B. Bally *et al.*, Imaging the initial condition of heavy-ion collisions and nuclear structure across the nuclide chart (2022), [arXiv:2209.11042 \[nucl-ex\]](https://arxiv.org/abs/2209.11042).
- [26] G. Gamow, *Constitution of Atomic Nuclei and Radioactivity* (Clarendon Press, 1931).
- [27] D. Brink *et al.*, Investigation of the alpha-particle model for light nuclei, *Phys. Lett. B* **33**, 143 (1970).
- [28] A. Tohsaki, H. Horiuchi, P. Schuck, and G. Röpke, Alpha cluster condensation in ^{12}C and ^{16}O , *Phys. Rev. Lett* **87**, 192501 (2001).
- [29] B. Zhou, Y. Funaki, H. Horiuchi, Y.-G. Ma, G. Röpke, P. Schuck, A. Tohsaki, and T. Yamada, The 5α condensate state in ^{20}Ne , *Nature Communications* **14**, 8206 (2023).
- [30] D. Bai, Z. Ren, and G. Röpke, α clustering from the quartet model, *Phys. Rev. C* **99**, 034305 (2019).
- [31] H. C. Manjunatha, N. Sowmya, P. S. D. Gupta, K. N. Sridhar, A. M. Nagaraja, L. Seenappa, and S. A. C. Raj, Investigation of decay modes of superheavy nuclei, *Nuc. Sci. Tech.* **32**, 130 (2021).
- [32] B. Buck, A. C. Merchant, and S. M. Perez, Systemat-

- ics of alpha-cluster states above double shell closures, *Phys. Rev. C* **51**, 559 (1995).
- [33] N. Itagaki, M. Ito, M. Milin, T. Hashimoto, H. Ishiyama, and H. Miyatake, Coexistence of $\alpha + \alpha + n + n$ and $\alpha + t + t$ cluster structures in ^{10}Be , *Phys. Rev. C* **77**, 067301 (2008).
- [34] C. J. Halcrow, C. King, and N. S. Manton, Dynamical α -cluster model of ^{16}O , *Phys. Rev. C* **95**, 031303 (2017).
- [35] L. Zhou, S.-M. Wang, D.-Q. Fang, and Y.-G. Ma, Recent progress in two-proton radioactivity, *Nucl. Sci. Tech.* **33**, 105 (2022).
- [36] M. A. Souza and H. Miyake, $\alpha + \text{core}$ structure described with an additional interaction in the nuclear matter saturation region, *Eur. Phys. J. A* **59**, 74 (2023).
- [37] L. Qin, K. Hagel, R. Wada, *et al.*, Laboratory Tests of Low Density Astrophysical Nuclear Equations of State, *Phys. Rev. Lett.* **108**, 172701 (2012).
- [38] W. B. He, Y. G. Ma, X. G. Cao, X. Z. Cai, and G. Q. Zhang, Giant Dipole Resonance as a Fingerprint of α Clustering Configurations in ^{12}C and ^{16}O , *Phys. Rev. Lett.* **113**, 032506 (2014).
- [39] W.-B. He, Q.-F. Li, Y.-G. Ma, Z.-M. Niu, J.-C. Pei, and Y.-X. Zhang, Machine learning in nuclear physics at low and intermediate energies, *Science China - Phys. Mech. Astro.* **66**, 282001 (2023).
- [40] W. B. He, Y. G. Ma, L. G. Pang, H. C. Song, and K. Zhou, Machine learning in nuclear physics at low and intermediate energies, *Nucl. Sci. Tech.* **34**, 88 (2023).
- [41] P. Bożek, W. Broniowski, E. R. Arriola, and M. Rybczyński, α clusters and collective flow in ultrarelativistic carbon-heavy-nucleus collisions, *Phys. Rev. C* **90**, 064902 (2014).
- [42] Y.-A. Li, S. Zhang, and Y.-G. Ma, Signatures of α -clustering in ^{16}O by using a multiphase transport model, *Phys. Rev. C* **102**, 054907 (2020).
- [43] C.-C. Guo, Y.-G. Ma, Z.-D. An, and B.-S. Huang, Influence of alpha-clustering configurations in $^{16}\text{O} + ^{197}\text{Au}$ collisions at Fermi energy, *Phys. Rev. C* **99**, 044607 (2019).
- [44] C. Z. Shi and Y. G. Ma, α clustering effect on flows of direct photons in heavy-ion collisions, *Nucl. Sci. Tech.* **32**, 66 (2021).
- [45] Y.-A. Li, D.-F. Wang, S. Zhang, and Y.-G. Ma, System scan of the multiplicity correlation between forward and backward rapidities in relativistic heavy-ion collisions using a multi-phase transport model, *Chin. Phys. C* **46**, 044101 (2022).
- [46] Y.-A. Li, D.-F. Wang, S. Zhang, and Y.-G. Ma, System evolution of forward-backward multiplicity correlations in a multiphase transport model, *Phys. Rev. C* **104**, 044906 (2021).
- [47] B. S. Huang, Y. G. Ma, and W. B. He, Photonuclear reaction as a probe for alpha-clustering nuclei in the quasi-deuteron region, *Phys. Rev. C* **95**, 034606 (2017).
- [48] B. S. Huang and Y. G. Ma, Two-proton momentum correlation from photodisintegration of α -clustering light nuclei in the quasi-deuteron region, *Phys. Rev. C* **101**, 034615 (2020).
- [49] B. S. Huang and Y. G. Ma, Dipole excitation of ^6Li and ^9Be studied with an extended quantum molecular dynamics model, *Phys. Rev. C* **103**, 054318 (2021).
- [50] M. Freer, H. Horiuchi, Y. Kanada-En'yo, D. Lee, and U.-G. Meissner, Microscopic clustering in light nuclei, *Rev. Mod. Phys.* **90**, 035004 (2018).
- [51] W. von Oertzen, M. Freer, and Y. Kanada-En'yo, Nuclear clusters and nuclear molecules, *Phys. Rep.* **432**, 43 (2006).
- [52] Y.-G. Ma, Effects of α -clustering structure on nuclear reaction and relativistic heavy-ion collisions, *Nucl. Tech. (in Chinese)* **46**, 080001 (2023).
- [53] W. Broniowski and E. Ruiz Arriola, Signatures of α Clustering in Light Nuclei from Relativistic Nuclear Collisions, *Phys. Rev. Lett.* **112**, 112501 (2014).
- [54] S. Zhang, Y. G. Ma, J. H. Chen, W. B. He, and C. Zhong, Nuclear cluster structure effect on elliptic and triangular flows in heavy-ion collisions, *Phys. Rev. C* **95**, 064904 (2017).
- [55] L. Ma, Y. G. Ma, and S. Zhang, Anisotropy fluctuation and correlation in central α -clustered $^{12}\text{C} + ^{197}\text{Au}$ collisions, *Phys. Rev. C* **102**, 014910 (2020).
- [56] Y.-Z. Wang, S. Zhang, and Y.-G. Ma, System dependence of away-side broadening and α -clustering light nuclei structure effect in dihadron azimuthal correlations, *Phys. Lett. B* **831**, 137198 (2022).
- [57] Z. W. Lin, C. M. Ko, B. A. Li, B. Zhang, and S. Pal, Multiphase transport model for relativistic heavy ion collisions, *Phys. Rev. C* **72**, 064901 (2005).
- [58] M. Souza, H. Miyake, T. Borello-Lewin, C. da Rocha, and C. Frajuca, α -Cluster structure above double-shell closures and α -decay of ^{104}Te , *Phys. Lett. B* **793**, 8 (2019).
- [59] G. Röpke, P. Schuck, Y. Funaki, H. Horiuchi, Z. Ren, A. Tohsaki, C. Xu, T. Yamada, and B. Zhou, Nuclear clusters bound to doubly magic nuclei: The case of ^{212}Po , *Phys. Rev. C* **90**, 034304 (2014).
- [60] Z.-W. Lin and L. Zheng, Further developments of a multiphase transport model for relativistic nuclear collisions, *Nucl. Sci. Tech.* **32**, 113 (2021).
- [61] X. N. Wang and M. Gyulassy, hijing: A Monte Carlo model for multiple jet production in pp, pA, and AA collisions, *Phys. Rev. D* **44**, 3501 (1991).
- [62] B. Zhang, ZPC 1.0.1: a parton cascade for ultrarelativistic heavy ion collisions, *Computer Physics Communications* **109**, 193 (1998).
- [63] B. Andersson, G. Gustafson, and B. Söderberg, A general model for jet fragmentation, *Z. Phys. C* **20**, 317 (1983).
- [64] T. Sjöstrand, High-energy-physics event generation with PYTHIA 5.7 and JETSET 7.4, *Comput. Phys. Commun.* **82**, 74 (1994).
- [65] B. A. Li and C. M. Ko, Formation of superdense hadronic matter in high energy heavy-ion collisions, *Phys. Rev. C* **52**, 2037 (1995).
- [66] M. A. Souza and H. Miyake, Search for $\alpha + \text{core}$ states in even-even Cr isotopes, *Eur. Phys. J. A* **53**, 146 (2017).
- [67] M. A. Souza and H. Miyake, Search for the $\alpha + \text{core}$ structure in the ground state bands of $22 \leq Z \leq 42$ even-even nuclei, *Phys. Rev. C* **104**, 064301 (2021).
- [68] Y. Funaki, A. Tohsaki, H. Horiuchi, P. Schuck, and G. Röpke, Analysis of previous microscopic calculations for the second 0^+ state in ^{12}C in terms of $3 - \alpha$ particle bose-condensed state, *Phys. Rev. C* **67**, 051306 (2003).
- [69] B. Zhou, Y. Funaki, H. Horiuchi, Z. Ren, G. Röpke, P. Schuck, A. Tohsaki, C. Xu, and T. Yamada, Non-localized Clustering: A New Concept in Nuclear Cluster Structure Physics, *Phys. Rev. Lett.* **110**, 262501 (2013).
- [70] W. Huang, M. Wang, F. Kondev, G. Audi, and S. Naimi, The AME 2020 atomic mass evaluation (I). Evaluation of input data, and adjustment procedures*, *Chinese Phys. C* **45**, 030002 (2021).

- [71] G. Röpke, L. Münchow, and H. Schulz, Particle clustering and Mott transitions in nuclear matter at finite temperature: (I). Method and general aspects, *Nucl. Phys. A* **379**, 536 (1982).
- [72] R. Wang, Y.-G. Ma, L.-W. Chen, C. M. Ko, K.-J. Sun, and Z. Zhang, Kinetic approach of light-nuclei production in intermediate-energy heavy-ion collisions, *Phys. Rev. C* **108**, L031601 (2023).
- [73] S. Yang, C. Xu, G. Röpke, P. Schuck, Z. Ren, Y. Funaki, H. Horiuchi, A. Tohsaki, T. Yamada, and B. Zhou, α decay to a doubly magic core in the quartetting wave function approach, *Phys. Rev. C* **101**, 024316 (2020).
- [74] C. Xu, Z. Ren, G. Röpke, P. Schuck, Y. Funaki, H. Horiuchi, A. Tohsaki, T. Yamada, and B. Zhou, α -decay width of ^{212}Po from a quartetting wave function approach, *Phys. Rev. C* **93**, 011306 (2016).
- [75] H.-C. Song, Y. Zhou, and K. Gajdošová, Collective flow and hydrodynamics in large and small systems at the LHC, *Nucl. Sci. Tech.* **28**, 99 (2017).
- [76] A. M. Poskanzer and S. A. Voloshin, Methods for analyzing anisotropic flow in relativistic nuclear collisions, *Phys. Rev. C* **58**, 1671 (1998).
- [77] Y. G. Ma, The Colective Flow from the Degree of Freedom of Nucleons to Quarks, *Journal of Fudan University (Natural Science)* **62**, 273 (2023).
- [78] M. Wang, J. Q. Tao, H. Zheng, W. C. Zhang, L. L. Zhu, and A. Bonasera, Number-of-constituent-quark scaling of elliptic flow: a quantitative study, *Nucl. Sci. Tech.* **33**, 37 (2022).
- [79] S. W. Lan and S. S. Shi, Anisotropic flow in high baryon density region, *Nucl. Sci. Tech.* **33**, 21 (2022).
- [80] H. Wang and J. H. Chen, Anisotropy flows in Pb-Pb collisions at LHC energies from parton scatterings with heavy quark trigger, *Nucl. Sci. Tech.* **33**, 15 (2022).
- [81] H.-X. Zhang, Y.-X. Xiao, J.-W. Kang, and B.-W. Zhang, Phenomenological study of the anisotropic quark matter in the two-flavor Nambu-Jona-Lasinio model, *Nucl. Sci. Tech.* **33**, 150 (2022).
- [82] V. Khachatryan *et al.* (CMS Collaboration), Evidence for collectivity in pp collisions at the LHC, *Phys. Lett. B* **765**, 193 (2017).
- [83] A. Bilandzic, R. Snellings, and S. Voloshin, Flow analysis with cumulants: Direct calculations, *Phys. Rev. C* **83**, 044913 (2011).
- [84] J. Jia, M. Zhou, and A. Trzupek, Revealing long-range multiparticle collectivity in small collision systems via subevent cumulants, *Phys. Rev. C* **96**, 034906 (2017).
- [85] Y. G. Ma and W. Q. Shen, Correlation functions and the disappearance of rotational collective motion in nucleus-nucleus collisions below 100 MeV/nucleon, *Phys. Rev. C* **51**, 3256 (1995).
- [86] S. Chatrchyan *et al.* (CMS Collaboration), Multiplicity and transverse momentum dependence of two- and four-particle correlations in pPb and PbPb collisions, *Phys. Lett. B* **724**, 213 (2013).
- [87] M. S. Abdallah *et al.* (STAR Collaboration), Search for the chiral magnetic effect with isobar collisions at $\sqrt{s_{NN}} = 200$ GeV by the STAR Collaboration at the BNL Relativistic Heavy Ion Collider, *Phys. Rev. C* **105**, 014901 (2022).
- [88] G. Aad *et al.* (ATLAS Collaboration), Centrality and rapidity dependence of inclusive jet production in sNN=5.02 TeV proton-lead collisions with the ATLAS detector, *Phys. Lett. B* **748**, 392 (2015).
- [89] S. Zhang, Y. G. Ma, G. L. Ma, J. H. Chen, Q. Y. Shou, W. B. He, and C. Zhong, Collision system size scan of collective flows in relativistic heavy-ion collisions, *Phys. Lett. B* **804**, 135366 (2020).
- [90] Z. Qiu and U. Heinz, Event-by-event shape and flow fluctuations of relativistic heavy-ion collision fireballs, *Phys. Rev. C* **84**, 024911 (2011).